A Finite Element Model of the Human Knee Joint for the Study of Tibio-Femoral Contact

Tammy L. Haut Donahue
Department of Mechanical Engineering,
Michigan Technological University,
Houghton, MI 49931

M. L. Hull*
Department of Mechanical Engineering,
and Biomedical Engineering Graduate Group,
University of California at Davis,
Davis, CA 95616

Mark M. Rashid
Associate Professor of Civil Engineering,
Department of Civil Engineering
University of California at Davis,
Davis, CA 95616

Christopher R. Jacobs
Associate Professor of Orthopaedics
Musculoskeletal Research Laboratory,
Penn State University,
Hershey, PA 17033

As a step towards developing a finite element model of the knee that can be used to study how the variables associated with a meniscal replacement affect tibio-femoral contact, the goals of this study were 1) to develop a geometrically accurate three-dimensional solid model of the knee joint with special attention given to the menisci and articular cartilage, 2) to determine to what extent bony deformations affect contact behavior, and 3) to determine whether constraining rotations other than flexion/extension affects the contact behavior of the joint during compressive loading. The model included both the cortical and trabecular bone of the femur and tibia, articular cartilage of the femoral condyles and tibial plateau, both the medial and lateral menisci with their horn attachments, the transverse ligament, the anterior cruciate ligament, and the medial collateral ligament. The solid models for the menisci and articular cartilage were created from surface scans provided by a noncontacting, laser-based, three-dimensional coordinate digitizing system with an root mean squared error (RMSE) of less than 8 microns. Solid models of both the tibia and femur were created from CT images, except for the most proximal surface of the tibia and most distal surface of the femur which were created with the three-dimensional coordinate digitizing system. The constitutive relation of the menisci treated the tissue as transversely isotropic and linearly elastic. Under the application of an 800 N compressive load at 0 degrees of flexion, six contact variables in each compartment (i.e., medial and lateral) were computed including maximum pressure, mean pressure, contact area, total contact force, and coordinates of the center of pressure. Convergence of the finite element solution was studied using three mesh sizes ranging from an average element size of 5 mm by 5 mm to 1 mm by 1 mm. The solution was considered converged for an average element size of 2 mm by 2 mm. Using this mesh size, finite element solutions for rigid versus deformable bones indicated that none of the contact variables changed by more than 2% when the femur and tibia were treated as rigid. However, differences in contact variables as large as 19% occurred when rotations other than flexion/extension were constrained. The largest difference was in the maximum pressure. Among the principal conclusions of the study are that accurate finite element solutions of tibio-femoral contact behavior can be obtained by treating the bones as rigid. However, unrealistic constraints on rotations other than flexion/extension can result in relatively large errors in contact variables. [DOI: 10.1115/1.1470171]

Introduction

Both complete and partial meniscectomies are performed in patients with torn menisci [1,2]. This procedure often causes degenerative arthritis in the knee [3–5]. Therefore, the efficacy of meniscal replacements in preventing the early onset of arthritis is of interest. To either design synthetic replacements, or select transplants that maintain normal contact on the tibial plateau, it is useful to identify independent variables (e.g., material properties) that are important determinants of the contact behavior of the tibio-femoral joint. A finite element model of the tibio-femoral joint that includes the menisci would be a powerful tool for making such identifications.

The human knee joint is a complex three-dimensional structure whose geometry is not easily represented by a solid model. Early finite element models used an axisymmetric representation of the knee [6–8]. However, axisymmetric models do not accurately represent the three-dimensional geometry of the femur-menisci-tibia complex. More recently, three-dimensional knee joint models, which include menisci, have been developed from images of cadaveric knees [9–11]. These models used either magnetic resonance imaging (MRI) [9,10] or reshaped digital calipers and machine–controlled contact digitization [11] to obtain soft tissue geometry. Both of these techniques have resolutions that are typically limited to 500 microns. Considering that the articular cartilage of the knee joint is only approximately 4 mm thick [12], a resolution of 500 microns is generally inadequate. For example, Li et al., [13] found that a 10% change in the thickness of the cartilage layer caused a corresponding 10% change in surface pressure in a model of the tibio-femoral joint. Therefore, the first goal of this study was to develop a three-dimensional solid geometric model from accurate digitized scans of the knee joint with special attention given to the menisci and articular cartilage.

Previous three-dimensional knee models have assumed that the femur and tibia were rigid [9–11]. To date, this assumption and its effects on the contact behavior of the tibio-femoral joint have not been investigated. An additional goal of the present study was to investigate the validity of treating the bones as rigid in relation to tibio-femoral contact.

Previous finite element studies have imposed unrealistic constraints on rotational degrees of freedom under compressive loading of the knee joint. In one study [11], varus-valgus (V/V) rotation was constrained, whereas in another study [10] movement of the femoral nodes with respect to the sagittal plane was constrained. In a third study, compressive translational displacements

*Corresponding author, e-mail: mlhull@ucdavis.edu

Contributed by the Bioengineering Division for publication in the JOURNAL OF BIOMECHANICAL ENGINEERING. Manuscript received by the Bioengineering Division June 26, 2000; revised manuscript received January 30, 2002. Associate Editor: G. A. Ateshian.

Fig. 1 Representative helical CT image used to obtain bone geometry with the points used for digitization. Solid lines represent the edges of the rods used for tissue geometry registration. Note that only one rod can be seen in this scan.

were applied thus constraining all rotational degrees of freedom to zero [9]. In reality, joint motion during compressive loading is coupled, so that fixing the rotational axis of the joint may impose abnormal motion [14]. Therefore, the last goal of this study was to show that constraints on joint motion affect the contact stress distribution of the joint during compressive loading.

Methods

A single right knee from a cadaveric specimen (male, age 30 years) was prepared for placement in a load application system to determine the functional axes in flexion/extension and axial rotation. Soft tissues within 10 cm of the joint line were left intact, whereas other tissues were removed. To interface the specimen with the load application system, steel rods, 12.5 mm in diameter, were inserted into the medullary canals of both the femur and tibia and cemented in place with polymethylmethacrylate (PMMA).

The knee was then aligned in the specialized load application system [15]. The knee was aligned using a functional axis approach that offers high repeatability [16]. Once the neutral position of the knee was determined, the knee was placed at 0 degrees of flexion. Two 5 mm in diameter delrin rods were then placed through the joint to fix this angle and allow registration of geometric data in post-processing. Delrin rods were used because they do not interfere with computer tomography scanning.

To image the bones, a helical computed tomography (CT) system was used to scan the knee in 0.5 mm increments in the frontal plane, from anterior to posterior at 0 degrees of flexion. The scan was performed in the frontal plane in order to maximize the resolution of the steeply inclined areas of the femoral condyles. The images of the slices were imported into Scion Image (Scion Corp., Frederick, MD) and the threshold was set to maximize contrast. This resulted in a pixel size of 500 microns by 500 microns for the 10 cm by 20 cm scan. The slices were manually digitized for both bone geometry and cortical shell thickness to 10 cm above and below the joint line. The two delrin rods that had been inserted through the joint at 0 degrees of flexion were also digitized to allow for registration of bony geometry with soft tissue geometry (Fig. 1).

Imaging of the soft tissues was achieved by using a laser-based three-dimensional coordinate digitizing system with a root mean squared error (RMSE) of less than 8 microns and a grid resolution of 0.5 mm by 0.5 mm [17]. The joint was disarticulated, and all soft tissues were removed except for the menisci and their ligamentous attachments. The exposed tibia/meniscus complex was scanned on the superior articulating surface, and on the medial, lateral, anterior, and posterior surfaces. The menisci were then removed and the tibial plateau was scanned. The tibial plateau was assumed to be congruent with the inferior surface of the menisci. These six scans provided the surface coordinate data from which the solid models of the menisci were reconstructed [17].

To reconstruct the articular cartilage, the tibia was placed in a 5.25% sodium hypochlorite solution for approximately 4 hours to remove cartilage down to the level of the tidemark [18]. The tibia was scanned to obtain the geometry of the tibial plateau without the cartilage. Cartilage thickness was determined by subtracting the scan without the cartilage from the scan with intact cartilage. A similar procedure was used to reconstruct the femoral cartilage. During the laser scanning, the two 5 mm in diameter delrin rods were exposed and scanned for registration with bony geometry.

The three-dimensional solid model of the knee specimen was developed by importing the local (x,y,z) coordinates from the digitized CT images and laser scanner into MSC/PATRAN (MacNiel-Schwindler Corp., Costa Mesa, CA). The various scans from the CT system and laser scanner were aligned using the two delrin rods. The centerline of each rod was used to define a 3-D vector. By transforming the two vectors from the CT data to align with the two vectors from the laser scanning, the images generated by the two different techniques were registered. A global coordinate system was established and all digitized data were transformed into the global system. The global coordinate system was established by first drawing a line parallel to the posterior osteochondral junction of the proximal tibia to define the medial-lateral (M/L) direction. The anterior-posterior (A/P) direction was defined as perpendicular to this line. The origin was placed at half the maximum A/P distance and half the maximum M/L distance.

To create a solid model suitable for finite element meshing, the digitized CT and laser-scanner data in the global coordinate system were connected using b-splines, generating 3-D curves. These curves were used to interpolate surfaces which in turn, defined the exterior faces of the 3D solid model. The solids were then exported from MSC/PATRAN and imported into TrueGrid (XYZ Scientific Applications Inc., Livermore, CA) which was used to automatically generate the mesh using 8-node continuum brick elements. The average element size in the initial mesh was 5 mm by 5 mm (or approximately 14 elements in the M/L direction and 7 elements in the A/P direction on the tibial plateau) and approximately 2 mm thick.

The material behavior of the cortical bone was assumed homogeneous and linearly elastic based on the level of loading and time duration of the load. Up to 10 cm from the joint line, the cortical shell can be considered homogenous [19]. Furthermore, because most of the change in the relaxation shear modulus $G(t)$ occurs after significant relaxation [20], it has been concluded that linear elasticity suffices as a constitutive relation for bone tissue in most situations involving physiological strains and strain rates [21,22].

Femoral cortical bone was modeled as orthotropic elastic using material constants derived from a study of the human femur (Table 1) [19]. Tibial cortical bone was modeled as orthotropic as well, but using different material constants reported in a study of the human tibia (Table 1) [23]. In both studies, direction 1 was radial, direction 2 was circumferential, and direction 3 was along the long axis of the bone.

Applying the same reasoning as with cortical bone [21,22], trabecular bone was also assumed to be linearly elastic and homogeneous. However, the material modulus for trabecular bone has been shown to be highly dependent on apparent density and location [24]. A study of the human femur showed that trabecular bone

Table 1 Orthotropic properties for cortical bone of both the femur [6] and the tibia [31]

	E_1 (GPa)	E_2 (GPa)	E_3 (GPa)	G_{12} (GPa)	G_{13} (GPa)	G_{23} (GPa)	ν_{12}	ν_{13}	ν_{23}
Femur	12.0	13.4	20.0	4.53	5.61	6.23	0.38	0.22	0.24
Tibia	6.9	8.5	18.4	2.4	3.6	4.9	0.49	0.12	0.14

near the joint surfaces is approximately isotropic and homogeneous [24]. Therefore, an average modulus of 0.4 GPa and a Poisson's ratio of 0.3 were used for trabecular bone in the present study.

Considering that the loading time of interest corresponds to that of a single leg stance, and that the viscoelastic time constant for cartilage approaches 1500 seconds, the cartilage was assumed to behave as a linearly elastic, isotropic, and homogeneous material for the purpose of analyzing contact stresses [25,26]. The elastic modulus ($E=15$ MPa) and Poisson ratio ($\nu=0.475$) values were selected based on direct measurements under short loading times [27].

An approach similar to that of previous studies [28–31] was used to model the ligaments of the knee joint. The following one-dimensional nonlinear relationship was employed:

$$f=k(\varepsilon-\varepsilon_1) \quad \text{if} \quad \varepsilon\geqslant 2\varepsilon_1$$

$$f=0.25k(\varepsilon^2/\varepsilon_1) \quad \text{if} \quad 0.0<\varepsilon<2\varepsilon_1$$

$$f=0 \quad \text{if} \quad \varepsilon\leqslant 0.0 \tag{1}$$

where ε is the strain in the ligament, ε_1 is the nonlinear strain level parameter assumed to be 0.03 as in previous studies [29,30,32], and k is the ligament stiffness. From Eq. (1) ligament force is assumed to bear a nonlinear relation to the extension for low strains, and a linear relation for strains higher than $2\varepsilon_1$. A previous study of the human knee joint loaded only in axial compression and at 0 degrees of flexion computed the force developed in each ligament [11]. Inasmuch as both the posterior cruciate and lateral collateral ligaments were slack under this compressive loading, only the anterior cruciate ligament (ACL) and medial collateral ligament (MCL) were included in the model. The ACL was represented by both anterior and posterior bundles, and the MCL was represented by both superficial and deep layers. The superficial layer was composed of three bundles—anterior, intermediate and posterior. The deep layer was composed of both anterior and posterior bundles. Values for the stiffness and reference strain were taken from the literature [29,30], where reference strain is the initial strain in the reference position (i.e., full extension). The attachment sites were determined from the laser scans of the tibia and femur. The ligaments were represented as nonlinear springs in the finite element model.

The incorporation of menisci into the model required both a constitutive description of the meniscal tissue, and a means of attachment both to the tibial plateau and to the surrounding structures. The menisci were modeled as linearly elastic, transversely isotropic with moduli of 20 MPa in the radial and axial directions [33–35], and 140 MPa in the circumferential direction [33–36]. The Poisson ratio in the plane of isotropy was 0.2, whereas the out-of-plane Poisson ratio was 0.3. The values for the Poisson ratios were taken from previous finite element studies [6–8,10]. The value for the horn stiffness was determined by using the modulus for ligament (111 MPa, [37]), and averaging the cross-sectional area (50 mm^2) and length (3 mm) of all four horns from the geometric model. This resulted in a value of 2000 N/mm. Each of the horns of the menisci was attached to the tibial plateau by ten linear springs, each with a stiffness of 200 N/mm, simulating the horn attachment. There were 10 nodes distributed over the part of each meniscus that was considered to be the horn (i.e., where the menisci attached to the plateau). The transverse ligament (TL) was modeled as a single linear spring with a stiffness of 200 N/mm because the area of the transverse ligament was small enough that only one node was in the vicinity of the attachment site.

The general-purpose finite element code ABAQUS (HKS Inc., Pawtucket, RI) was used to obtain approximate solutions to the problem. The bone, articular cartilage, and menisci were discretized into 8-node trilinear hexahedral elements. Hexahedral elements were chosen over tetrahedral elements despite the attending difficulties in automatic mesh generation. The model was run on a KryoTech 767au workstation (Kryotech, West Columbia, SC).

Contact was modeled between the femur and meniscus, the meniscus and tibia, and the femur and tibia for both the lateral and medial hemijoints, resulting in six contact-surface pairs. The contact conditions in the model were completely general involving finite sliding of pairs of curved, deformable surfaces. Obtaining high-quality computational solutions under these general conditions represented a significant challenge. All of the surfaces were modeled as frictionless. The contact pressure-clearance relationship used to define the surface interaction was a ''hard'' contact model, in the sense that no penetration was allowed of the nodes from one surface into the other surface, and no transfer of tensile stress was allowed across the interface. A slave and master surface were defined for each contact pair set (i.e., femur and meniscus, meniscus and tibia, tibia and femur). Each slave node was checked for penetration into its corresponding master surface. A measure of penetration, or ''overclosure,'' into the master surface was defined for each slave node. The overclosure was constrained to be nonpositive at each slave node. As a result, unknown nodal forces were introduced in the weak statement of equilibrium and were solved for in the equilibrium iteration. These nodal forces played the role of Lagrange multipliers conjugate to the overclosure constraint.

Convergence of the equilibrium iteration was assessed based on two separate criteria. In the first, the maximum residual nodal force was required to be less than a user-defined fraction of a spatially and temporally averaged force for the entire structure. In the calculations reported herein, the fraction was taken to be 0.5%. In the second, independent convergence criterion, the last iterative correction to the incremental nodal displacement was required to be less than 1% of the incremental nodal displacement itself at each node. On each Newton iteration, the nonpositive overclosure constraint was enforced. A successful load step was achieved when both of the above-mentioned convergence criteria were satisfied.

During compressive loading, all three rigid-body translations and rotations of the proximal femur were fixed, whereas the distal tibia was constrained only in flexion/extension (F/E). A compressive force of 800 N (1 body weight) was applied through the distal tibia at 0 degrees of flexion. Six contact-related variables were determined: 1) maximum pressure, 2) mean pressure, 3) total

Table 2 Lateral and medial contact variables for the three finite element mesh densities. Center of pressure coordinates are referenced to the global coordinate system, with positive being anterior and medial for A/P and M/L respectively.

LATERAL

Average element size	Max. Pressure (MPa)	Mean Pressure (MPa)	Total Force (N)	Area (mm^2)	A/P-coordinate of center of pressure (mm)	M/L-coordinate of center of pressure (mm)
5 mm by 5 mm	3.05	1.02	410	365	-3.5	-16.2
2 mm by 2 mm	2.38	0.88	404	409	-5.2	-18.9
1 mm by 1 mm	2.36	0.88	408	415	-5.4	-18.5

MEDIAL

Average element size	Max. Pressure (MPa)	Mean Pressure (MPa)	Total Force (N)	Area (mm^2)	A/P-coordinate of center of pressure (mm)	M/L-coordinate of center of pressure (mm)
5 mm by 5 mm	2.75	1.16	415	410	0.6	32.6
2 mm by 2 mm	2.51	0.80	411	483	-4.4	34.1
1 mm by 1 mm	2.55	0.78	409	490	-4.0	34.3

force due to contact pressure, 4) area of contact, and 5) and 6) the anterior/posterior (A/P) and medial/lateral (M/L) locations of the center of pressure.

To test for model convergence, the contact variables were recorded for each of three mesh sizes. The initial mesh, with an average element size of 5 mm by 5 mm (approximately 14 elements M/L and 7 elements A/P on the tibial plateau) over the surfaces of contact, was refined to a mesh with an average element size of 2 mm by 2 mm (approximately 35 elements M/L and 18 elements A/P on the tibial plateau) over the contact surfaces. A third and final mesh was generated with an average element size of 1 mm by 1 mm (approximately 70 elements M/L and 35 elements A/P on the tibial plateau). In addition, the number of elements through the thickness of the cartilage, menisci, and subchondral bone was increased from 2 to 3 to 4 elements with increasing mesh density.

Separate simulations were performed with the bones modeled as both deformable and as rigid to determine the validity of the rigid-bone assumption. To make the bones rigid, rigid surfaces were attached to the proximal side of the femoral cartilage and to the distal side of the tibial cartilage. Making the bones rigid also involved transection of the superficial medial collateral ligament, because there was no longer deformable bone, with its nodes, at the attachment site of the superficial MCL. However, the deep MCL was retained and the attachment of the nonlinear spring was moved to the rigid surface.

To investigate the effect of boundary conditions on joint contact, the following additional analyses were performed with different rotational constraints on the tibia: 1) only F/E rotation constrained, 2) both F/E rotation and varus/valgus rotation (V/V) constrained, 3) both F/E rotation and internal/external rotation (I/E) constrained, and 4) all three tibial rotational degrees of freedom constrained.

Results

A three-dimensional solid model of the entire tibio-femoral joint was constructed and meshed. All surfaces in contact were scanned with an RMSE of less than 8 microns. Because a surface subtraction technique was used to obtain tissue thickness, the maximum error possible was less than 16 microns in the surface coordinates used to generate the solid model.

The convergence test indicated that the finite element solution was accurate for the intermediate mesh size of 2 mm by 2 mm (approximately 35 mm M/L and 18 elements A/P on the tibial plateau). Increasing the mesh from the intermediate element size to the largest mesh size of 5 mm by 5 mm changed all but one of the contact variables by up to 45% relative to the results for the intermediate mesh size (Table 2). For the coordinates of the center of pressure, the maximum change was 3 mm for the A/P-coordinate in the medial compartment. Decreasing the mesh to the smallest size of 1 mm by 1 mm changed the contact variables (other than the coordinates of the center of pressure) by 2.5% at most. Therefore, the second mesh was judged sufficiently fine, and was used as the reference size for the remainder of the study. The final mesh, with an average element size of 2 mm by 2 mm, consisted of 14,050 total elements: 2500 meniscal elements in four layers, 3000 femoral cartilage elements in four layers, 2500 tibia cartilage elements in four layers, and 6000 cortical and trabecular bone elements for the femur and tibia (Fig. 2). The load was applied in 10 increments and contact was the primary source of nonlinearity in the problem (Fig. 3).

When the bones were assumed rigid, the percent change in any one contact variable was always less than 2% in each compartment (Table 3). This assumption eliminated approximately 5000 finite elements (Fig. 4), and reduced the running time by 50% (4 hours), resulting in a total run time of approximately 4 hours.

Constraining rotations in addition to F/E rotation caused changes in the maximum pressure at 800 N (1 BW) relative to that with only F/E rotation constrained. With all three rotations constrained, the maximum pressure decreased 5% (from 2.38 to 2.25 MPa) on the lateral side and 16% (from 2.51 to 2.10 MPa) on the medial side (Table 3). When either V/V rotation or I/E rotation was constrained, the maximum pressure increased on the lateral side by 9% and 2%, respectively. However, on the medial side, when either V/V rotation or I/E rotation was constrained, the maximum pressure decreased by 19% and 16%, respectively.

Constraining rotations in addition to F/E rotation also caused changes in the mean pressure relative to that with only F/E rotation constrained. With V/V rotation constrained, the mean pressure on the lateral side increased by 7%, but if either I/E rotation or V/V rotation and I/E rotation were constrained, then the mean pressure decreased by 6% and 3% respectively. As additional rotations were constrained, the mean pressure decreased on the medial side by 11%, 9%, and 4% with V/V rotation constrained, I/E rotation constrained, and both V/V rotation and I/E rotation constrained, respectively (Table 3).

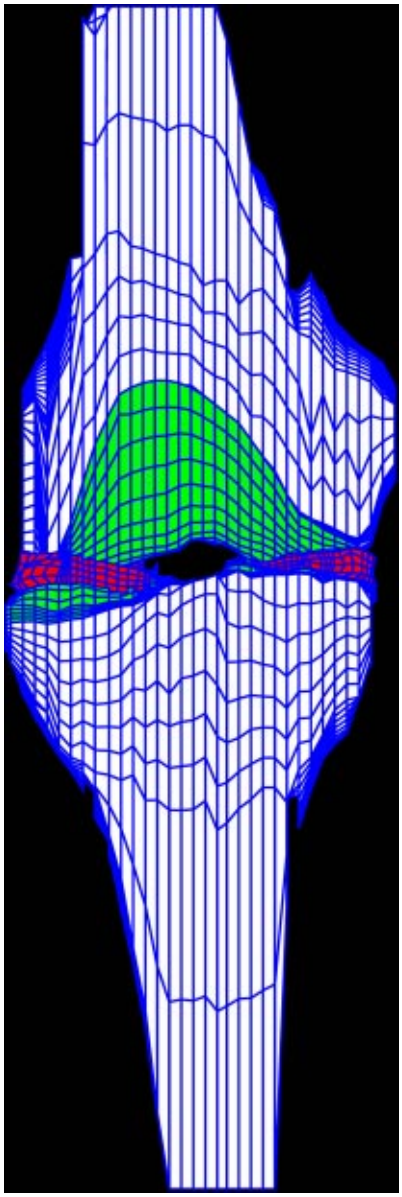

Fig. 2 Anterior view of the finite element representation of the entire tibio-femoral joint (ligaments and meniscal attachments removed for clarity)

These results indicate the load transmission shifted between the two compartments when rotations in addition to F/E rotation were constrained. Load transmission shifted from the medial to the lateral tibial plateau when V/V rotation was constrained in addition to F/E rotation. The total force due to contact increased on the lateral side by 14%. This was mirrored by a decrease in total contact force on the medial side by 15% (Table 3). When I/E rotation was constrained, the total contact force on the lateral side changed by less than 1.5%, and the total contact force on the medial side decreased by approximately 7%. When both V/V rotation and I/E rotation were constrained, the total force increased approximately 4% on the lateral side and decreased approximately 7% on the medial side.

Lateral and medial contact areas were minimally affected when any of the other rotations were constrained in addition to F/E rotation (Table 3). On the lateral side, with any other rotation constrained, the contact area increased by about 3–4%. On the medial side, the only notable difference in contact area occurred when V/V rotation was constrained (4% increase).

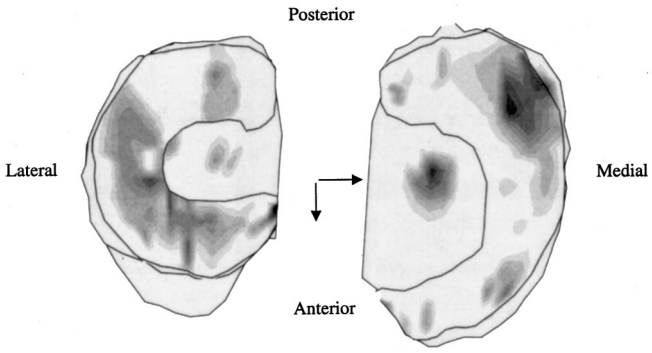

Fig. 3 Contact pressure pattern from the tibial plateau under 800 N compressive force at 0 degrees flexion, deformable bones, the intermediate mesh size, and F/E constrained

The location of the center of pressure shifted slightly mediposteriorly on the lateral tibial plateau as rotations were constrained in addition to F/E rotation. There was a 1 mm shift in the medial direction, and about a 0.4 mm shift in the posterior direction (Table 3). In the medial hemijoint, the largest shifts of 0.4 mm in the medial direction and 0.2 mm in the anterior direction occurred when V/V rotation was constrained (Table 3).

Discussion

The underlying motivation for this study was to develop a computational tool that could ultimately be used to identify variables important in the design and/or selection of meniscal replacements. The specific objectives of this study were to 1) create a solid model of the human knee joint from accurate three-dimensional digitized scans, particularly the soft tissues, 2) determine to what extent bony deformations affect contact behavior, and 3) determine the effects of rotational constraints. The key findings from the study were that 1) a solid model for the soft tissues can successfully be used to study the contact behavior of the knee joint with the finite element method, 2) bony deformations did not significantly affect the contact behavior up to 1 body weight at 0 degrees of flexion and 3) rotational constraints caused changes as large as 19% in contact variables. Issues related to each of these findings will be discussed in turn.

Although the soft tissue geometry, as well as the proximal surface of the tibia's subchondral bone, and the distal surface of the femoral subchondral bone, were obtained from a noncontacting three-dimensional coordinate digitizing system with an RMSE of less than 8 microns, the actual error in the soft tissues in the solid model may have been larger for three reasons. First, the laser-based scanning process required 30 minutes, which may have caused some degree of tissue dehydration [17]. If dehydration occurred, then the volume of both the menisci and cartilage would have been underestimated. Second, the congruence of the tibia with the inferior surface of the meniscus was assumed. If the two surfaces were not congruent, then the height of the menisci along the direction normal to the tibial plateau would have been overestimated. Third, the accuracy of the solid model also depends on the level of fidelity with which the solid model fit the digitized points. Considering that the various articulating surfaces scanned to generate the solid model were smooth, this latter error is expected to be minimal.

Because the noncontacting three-dimensional coordinate digitizing system could not be used to obtain either the subchondral bone thickness or the remaining portion of the femur and tibia, CT images were used for obtaining this geometry. While the thickness of the subchondral bone was not constant in this study, it was approximately 3–4 mm thick. Inasmuch as the surfaces of the bones were scanned with the coordinate digitizing system, with an RMSE of less than 8 microns, and the inner surface of the sub-

Table 3 Lateral and medial contact variables at 800 N (1 BW) for rigid and deformable bones and the various rotational constraints. Center of pressure coordinates are referenced to the global coordinate system, with positive being anterior and medial for A/P and M/L respectively.

LATERAL

Constrained DOF	Max. Pressure (MPa)	Mean Pressure (MPa)	Total Force (N)	Area (mm^2)	A/P-coordinate of center of pressure (mm)	M/L-coordinate of center of pressure (mm)
Rigid bones, F/E	2.35	0.88	401	411	-5.3	-18.9
F/E	2.38	0.88	404	409	-5.2	-18.9
F/E, V/V	2.60	0.94	461	422	-5.3	-18.6
F/E, I/E	2.43	0.83	401	419	-5.6	-17.9
F/E, V/V, I/E	2.25	0.85	424	424	-5.5	-17.9

MEDIAL

Constrained DOF	Max. Pressure (MPa)	Mean Pressure (MPa)	Total Force (N)	Area (mm^2)	A/P-coordinate of center of pressure (mm)	M/L-coordinate of center of pressure (mm)
Rigid bones, F/E	2.50	0.82	409	489	-4.4	34.2
F/E	2.51	0.80	411	483	-4.4	34.1
F/E, V/V	2.04	0.72	351	463	-4.2	34.5
F/E, I/E	2.10	0.73	383	483	-4.3	34.1
F/E, V/V, I/E	2.10	0.77	389	483	-4.3	34.2

chondral bone was digitized from the CT images with a resolution of only 500 microns, there is potential for errors as large as 508 microns through the thickness of the subchondral bone (a 13% error). This poor resolution was a result of the large scan area per slice of 20 cm by 10 cm for the CT images. However, it is unlikely that this error affected our results considering that contact variables changed by less than 2% when the bones were assumed rigid.

Once a solid geometric model has been created, the model must be meshed. Two of the three-dimensional finite element knee joint models previously reported used very coarse meshes on the order of 800 elements for all of the soft tissues [9,11]. Neither study involved any analysis to determine if the finite element solution was converged. The current model was meshed from a geometric model that was more accurate than previous models, the mesh size was the smallest, and the solution was demonstrated to have converged for this mesh size.

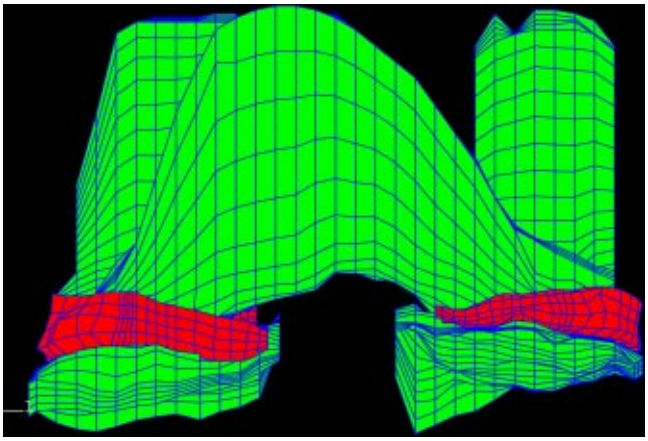

Fig. 4 Anterior view of the finite element representation of the joint with the assumption of rigid bones

The mesh size is also related to how well the hexahedral finite element mesh approximates the solid model. In general the surface of the discretized finite element mesh does not match that of the solid model [38]. Although distances between these surfaces have been shown potentially to be sizable [39], the small finite element mesh size in conjunction with the smoothness of the surfaces in the solid model reduced these differences.

To achieve the objectives of the study, contact variables of the tibial plateau were investigated since the efficacy of meniscal replacements in preventing the early onset of arthritis is of interest ultimately. While increased contact stresses have been hypothesized to lead to osteoarthritis [40,41], meniscal displacements and motion have not been directly linked to osteoarthritis previously and the interpretation of changes in these quantities would be difficult to assess. Also, while changes may occur in either the motion or displacement of the meniscal replacement compared to the native meniscus, it is ultimately the cartilage that breaks down during osteoarthritis. Hence, the altered loading state that the cartilage may experience due to changes in meniscal quantities (e.g., material and geometry parameters) that affect contact was of primary interest. Also while we chose to investigate the surface stresses rather than internal stresses, both may be important to the degradation of articular cartilage.

The cartilage material behavior was considered to be linearly elastic rather than biphasic. It has been shown that the fluid within the tissue does not have time to move for short loading times (i.e., less than 1 second). Thus, the elastic solution does not deviate from the biphasic solution for these short loading times [42]. This simplified representation of the cartilage material behavior did not affect the results of this study because the resultant boundary tractions are the same for short loading times for both single-phase and biphasic materials [43].

Currently, the model does not include the patellofemoral joint. Including the patellofemoral joint would increase the complexity of the contact by adding another contact surface, hence leading to an increase in the run time. Because the contact behavior of the tibio-femoral joint under a compressive load at 0 degrees of flex-

ion was of interest, the patellofemoral joint was not included in the current version of the model. Of course, this joint could be added if the application required it.

While no patellofemoral joint was included in the model, the structures that have been shown previously to be important under compressive loading of the tibio-femoral joint were included, in addition to the attachments of the menisci. Both the ACL and MCL were included in the model, because they have been shown previously to be in tension when a compressive load was applied to the knee joint at 0 degrees of flexion [11].

On the other hand, both the lateral collateral ligament (LCL) and posterior cruciate ligament (PCL) were not included. Although these ligaments have been shown to be slack under compressive loading at 0 degrees of flexion [11], rotational constraints other than F/E were applied to the model in that study. Accordingly to check that these ligaments did not come into play during the unconstrained coupled motions that occurred when only F/E was constrained in the present study, their influence on joint contact was assessed by solving the model both with and without these ligaments. The ligaments were modeled as nonlinear springs [30,31]. The root mean squared difference in the contact variables was only 0.91 when comparing the model solution with the PCL and LCL to the model solution without these ligaments. The less than 1% change indicates that these ligaments do not influence joint contact behavior even when the joint is unconstrained.

The attachments of the menisci to the tibial plateau, and to each other via the transverse ligament, were included in the model. Furthermore, the medial meniscus attachment to the deep medial collateral ligament was included. Each of these structures stretched under the applied compressive load in this model. Again, the present three-dimensional model is the first that we know of that included all of these attachments.

Although the finite element solution may have converged indicating that the finite element solution was accurate, confidence in the validity of the model itself (as opposed to its numerical solution) can be gained by comparing the values of the contact variables to previously reported experimental data. Of the many studies that have measured contact pressure on the tibial plateau [44–50], the study by Huang provided the data most relevant for a meaningful comparison to the data from the present study. This is because Huang used a load application system that applied compressive load of 800 N with all other degrees of freedom except F/E unconstrained, and computed the maximum pressure, the mean pressure, and contact area thus enabling a direct comparison with the results from the present study for the lateral tibial plateau. The ± 2 standard deviation ranges for the contact variables were 1.6–7.2 MPa for the maximum pressure, 0.7–3.5 MPa for the mean pressure, and 135–475 mm^2 for the contact area. Inasmuch as the maximum pressure of 2.35 MPa, mean pressure of 0.88 MPa, and contact area of 411 mm^2 obtained from the present study all fall well within these ranges, the values of contact variables provided by the model are within normal limits for knees. Therefore, it is reasonable to expect that the relative differences seen in the present study would be representative of those for human knee joints as well.

This analysis demonstrated that the assumption of rigid bones is valid when computing contact variables of the tibial plateau up to 1 body weight. While all three previous 3-D finite element models of the tibio-femoral joint that included menisci [9–11] made the assumption of rigid bones, this study is the first to investigate the validity of this assumption. The rigid-bone assumption reduced the computational time by approximately 50% (i.e. from 8 hours to 4 hours).

This study also showed that the superficial MCL has little effect on the contact variables. The change in contact variables seen with the bones assumed rigid, which involved deleting the superficial MCL from the model, was less than 2%. In view of this negligible change, we did not investigate whether the change was due either to rigid bones or to the loss of the MCL.

Because the contact variables were quite sensitive to the rotational constraints imposed on the model, it is important to know the rotational constraints as well as the loads transmitted by the joint during an activity of interest (e.g., walking) to achieve an accurate picture of tibio-femoral contact. While the rotations are not constrained to zero during walking, some amount of constraint would be expected due to muscle forces and ground contact. The problem then becomes one of identifying the appropriate constraints to place on the joint. In this connection it bears mention that many gait studies have demonstrated large coupled motions of up to 20 degrees of rotation in both the V/V and I/E degrees of freedom [51–53]

In conclusion, this study provides a simplified yet geometrically accurate model of the human knee joint for studying tibio-femoral contact behavior. The convergence study demonstrated the importance of appropriately refining mesh size, as up to a 45% change in contact variables occurred from one mesh density to the next. Moreover, the study of rigid bones indicated that this assumption is valid when the contact behavior of cartilagenous joints are of interest. Substantial savings in computer solution time are possible with this assumption. Finally the contact behavior of the knee joint is sensitive to rotational constraints placed on the joint. Therefore, future studies should pay special attention to the rotational constraints applied to the joint during compressive loading, because changes as large as 19% were found in this study. Because we were able to generate an accurate finite element model of the tibio-femoral joint that includes the menisci, this model can be used for future studies that will identify the meniscal variables, such as material properties, geometry, and boundary conditions, that are important determinants of contact behavior.

Acknowledgment

The authors are grateful to the Whitaker Foundation for providing the financial support to undertake this project.

References

[1] Newman, A. P., Daniels, A. U., and Burks, R. T., 1993, ''Principles and Decision Making in Meniscal Surgery,'' Arthroscopy, **9**, pp. 33–51.
[2] Siegel, M. G., and Roberts, C. S., 1993, ''Meniscal Allografts,'' Clin. Sports Med., **12**, pp. 59–80.
[3] Rangger, C., Klestil, T., Gloetzer, W., Kemmler, G., and Benedetto, L. P., 1995, ''Osteoarthritis After Arthroscopic Partial Meniscectomy,'' Am. J. Sports Med., **23**, pp. 240–244.
[4] Fauno, P., and Nielson, A. B., 1992, ''Arthroscopic Partial Meniscectomy: A Long Term Follow-Up,'' Arthroscopy, **8**, pp. 345–349.
[5] Bolano, L. E., and Grana, W. A., 1993, ''Isolated Arthroscopic Partial Meniscectomy: Functional Radiographic Evaluation at Five Years,'' Am. J. Sports Med., **21**, pp. 432–437.
[6] Aspden, R. M., 1985, ''A Model for the Function and Failure of the Meniscus,'' Eng. Med., **14**, pp. 119–122.
[7] Hefzy, M. S., Grood, E. S., and Zoghi, M., 1987, ''An Axisymmetric Finite Element Model of the Meniscus,'' in *1987 Advances in Bioengineering*, American Society of Mechanical Engineers, New York, pp. 51–52.
[8] Schreppers, G. J. M. A., Sauren, A. A. H. J., and Huson, A., 1990, ''A Numerical Model of the Load Transmission in the Tibio-Femoral Contact Area,'' Journal of Engineering in Medicine, **204**, pp. 53–59.
[9] Zhang, H., Totterman, S., Perucchio, R., and Lerner, A. L., 1999, ''Magnetic Resonance Image Based 3D Poroelastic Finite Element Model of Tibio-Menisco-Femoral Contact,'' in *23rd Proceedings of the American Society of Biomechanics*, Pittsburgh, PA, pp. 198–199.
[10] Perie, D., and Hobatho, M. C., 1998, ''In Vivo Determination of Contact Areas and Pressure of the Femorotibial Joint Using Non-Linear Finite Element Analysis,'' Clin. Biomech., **13**, pp. 394–402.
[11] Bendjaballah, M. Z., Shirazi-Adl, A., and Zukor, D. J., 1995, ''Biomechanics of the Human Knee Joint in Compression: Reconstruction, Mesh Generation and Finite Element Analysis,'' The Knee, **2**, pp. 69–79.
[12] Froimson, M. I., Ateshian, G. A., Soslowsky, L. J., Kelly, M. A., and Mow, V. C., 1989, ''Quantification of the Surfaces at the Patellofemoral Articulation,'' Proc. Inst. Mech. Eng. [H], **5**, pp. 73–78.
[13] Li, G., and Loopez, O., 1999, ''Reliability of a 3D Finite Element Model Constructed Using Magnetic Resonance Images of a Knee for Joint Contact Stress Analysis,'' in *23rd Proceedings of the American Society of Biomechanics*, Pittsburgh, PA, pp. 196–197.
[14] Andriacchi, T. P., Mikosz, R. P., Hampton, S. J., and Galante, J. O., 1983, ''Model Studies of the Stiffness Characteristics of the Human Knee Joint,'' J. Biomech., **16**, pp. 23–29.

[15] Bach, J. M., and Hull, M. L., 1995, ''A New Load Application System for In Vitro Study of Ligamentous Injuries to the Human Knee Joint,'' J. Biomech. Eng., **117**, pp. 373–382.
[16] Berns, G. S., Hull, M. L., and Patterson, H. A., 1990, ''Implementation of a Five Degree of Freedom Automated System to Determine Knee Flexibility in Vitro,'' J. Biomech. Eng., **112**, pp. 392–400.
[17] Haut, T. L., Hull, M. L., and Howell, S. M., 1997, ''A High Accuracy Three-Dimensional Coordinate Digitizing System for Reconstructing the Geometry of Diarthrodial Joints,'' J. Biomech., **31**, pp. 571–577.
[18] Ateshian, G. A., Soslowsky, L. J., and Mow, V. C., 1991, ''Quantitation of Articular Surface Topography and Cartilage Thickness in Knee Joints Using Stereophotogrammetry,'' J. Biomech., **24**, pp. 761–776.
[19] Ashman, R. B., Cowin, S. C., Van Bruskirk, W. C., and Rice, J. C., 1984, ''A Continuous Wave Technique for the Measurement of the Elastic Properties of Bone,'' J. Biomech., **17**, pp. 349–361.
[20] Lakes, R. S., and Katz, J. L., 1979, ''Viscoelastic Properties of Wet Cortical Bone. III. A Non-linear Constitutive Equation,'' J. Biomech., **12**, pp. 689–698.
[21] Cowin, S. C., 1989, ''The Mechanical Properties of Cortical Bone Tissue,'' in *Bone Mechanics*, S. C. Cowins, ed., CRC Press, Boca Raton, FL, pp. 98–127.
[22] Cowin S. C., 1989, ''The Mechanical Properties of Cancellous Bone,'' in *Bone Mechanics*, S. C. Cowins, eds., CRC Press, Boca Raton, FL, pp. 129–157.
[23] Knets, I., and Malmeister, A., 1977, ''Deformability and Strength of Human Compact Bone Tissue,'' *Mechanics of Biological Solids*, Bulgarian Academy of Sciences, pp. 133.
[24] Kuhn, J. L., Goldstein, S. A., Ciarelli, M. J., and Matthews, L. S., 1989, ''The Limitations of Canine Trabecular Bone as a Model for Human: A Biomechanical Study,'' J. Biomech., **22**, pp. 95–107.
[25] Armstrong, C. G., Lai, W. M., and Mow, V. C., 1984, ''An Analysis of the Unconfined Compression of Articular Cartilage,'' J. Biomed. Eng., **106**, pp. 165–173.
[26] Eberhardt, A. W., Keer, L. M., Lewis, J. L., and Vithoontien, V., 1990, ''An Analytical Model of Joint Contact,'' J. Biomech. Eng., **112**, pp. 407–413.
[27] Shepard, D. E. T., and Seedhom, B. B., 1999, ''The 'Instantaneous' Compressive Modulus of Human Articular Cartilage in Joints of the Lower Limb,'' Rheumatology, **38**, pp. 124–132.
[28] Wismans, J., Veldpaus, F., Janssen, J., Huson, A., and Struben, P., 1980, ''A Three-Dimensional Mathematical Model of the Knee Joint,'' J. Biomech., **13**, pp. 677–685.
[29] Pandy, M. G., Sasaki, K., and Kim, S., 1997, ''A Three-Dimensional Musculoskeletal Model of the Human Knee Joint. Part I: Theoretical Construction,'' Computer Methods in Biomedical Engineering, **1**, pp. 87–108.
[30] Li, G., Gil, J., Kanamori, A., and Woo, S. L., 1999, ''A Validated Three-Dimensional Computational Model of a Human Knee Joint,'' J. Biomech. Eng., **121**, pp. 657–662.
[31] Blankevoort, L., Kuiper, J. H., Huiskes, R., and Grootenboer, H. J., 1991, ''Articular Contact in a Three-Dimensional Model of the Knee,'' J. Biomech., **24**, pp. 1019–1031.
[32] Butler, D. L., Kay, M. D., and Stouffer, D. C., 1986, ''Comparison of Material Properties in Fascicle-Bone Units from Human Patellar Tendon and Knee Ligaments,'' J. Biomech., **19**, pp. 425–432.
[33] Tissakht, M., and Ahmed, A. M., 1995, ''Tensile Stress-Strain Characteristics of the Human Meniscal Material,'' J. Biomech., **28**, pp. 411–422.
[34] Skaggs, D. L., Warden, W. H., and Mow, V. C., 1994, ''Radial Tie Fibers Influence the Tensile Properties of the Bovine Medial Meniscus,'' J. Orthop. Res., **12**, pp. 176–185.
[35] Whipple, R., Wirth, C. R., and Mow, V. C., 1984, ''Mechanical Properties of the Meniscus,'' in *1984 Advances in Bioengineering*, American Society of Mechanical Engineers, New York, pp. 32–33.
[36] Fithian, D. C., Schmidt, M. B., Ratcliffe, A., and Mow, V. C., 1989, ''Human Meniscus Tensile Properties: Regional Variation and Biochemical Correlation,'' in *Transactions of the Orthopedic Research Society*, **35**, pp. 205.
[37] Noyes, F. R., and Grood, E. S., 1976, ''The Strength of the Anterior Cruciate Ligament in Humans and Rhesus Monkeys,'' J. Bone Jt. Surg., Am. Vol., **58**, pp. 1074–1082.
[38] Merz, B., Niederer, P., Muller, R., and Ruegsegger, P., 1996, ''Automated Finite Element Analysis of Excised Human Femora Based on Precision-QCT,'' J. Biomech. Eng., **118**, pp. 387–390.
[39] Viceconti, M., Bellingeri, L., Cristofolini, L., and Toni, A., 1998, ''A Comparative Study on Different Methods of Automatic Mesh Generation of Human Femurs,'' Med. Eng. Phys., **20**, pp. 1–10.
[40] Allen, P. R., Denham, R. A., and Swan, A. V., 1984, ''Late Degenerative Changes After Meniscectomy. Factors Affecting the Knee after Operation,'' J. Bone Jt. Surg. Br. Vol. **66**, pp. 666–671.
[41] Howell, D. S., Treadwell, B. B., and Trippel, S. B., 1992, ''Etiopathogenesis of Osteoarthritis,'' in *Osteoarthritis, Diagnosis and Medical/Surgical Management*, R. W. Moskowitz, Howell, D. S., Goldberg, V. M., Mankin, H. J., eds., WB Saunders, Philadelphia, PA.
[42] Donzelli, P. S., Spilker, R. L., Ateshian, G. A., and Mow, V. C., 1999, ''Contact Analysis of Biphasic Transversely Isotropic Cartilage Layers and Correlations with Tissue Failure,'' J. Biomech., **32**, pp. 1037–1047.
[43] Garcia, J. J., Altiero, N. J., and Haut, R. C., 1998, ''An Approach for the Stress Analysis of Transversely Isotropic Biphasic Cartilage Under Impact Load,'' J. Biomech. Eng., **120**, pp. 608–613.
[44] Ahmed, A. M., and Burke, D. L., 1983, ''In-vitro Measurement of Static Pressure Distribution in Synovial Joints-Part I: Tibial Surface of the Knee,'' J. Biomech. Eng., **105**, pp. 216–225.
[45] Alhalki, M. M., Howell, S. M., and Hull, M. L., 1999, ''How Three Methods for Fixing a Medial Meniscal Autograft Affect Tibial Contact Mechanics,'' Am. J. Sports Med., **27**, pp. 320–328.
[46] Fukubayashi, T., and Kurosawa, H., 1980, ''The Contact Area and Pressure Distribution Pattern of the Knee. A Study of Normal and Osteoarthritic Knee Joints,'' Acta Orthop. Scand., **51**, pp. 871–879.
[47] Huang, A. Z., 2000, ''Cross-sectional Parameters of Lateral Meniscal Allografts that Determine the Differences in Tibial Contact Mechanics from the Intact Meniscus in Cadaveric Knees,'' MS Thesis in Biomedical Engineering, University of California at Davis, Davis, CA.
[48] Paletta, G. A., Manning, T., Snell, E., Parker, R., and Bergfeld, J., 1997, ''The Effect of Allograft Meniscal Replacement on Intraarticular Contact Area and Pressures in the Human Knee,'' Am. J. Sports Med., **25**, pp. 692–698.
[49] Sekaran, V., Hull, M. L., and Howell, S. M., 2002, ''Non-anatomic Location of the Posterior Horn of the Medial Meniscal Autograft Implanted in a Cadaveric Knee Adversely Affects the Pressure Distribution on the Tibial Plateau,'' Am. J. Sports Med., **30**, pp. 74–82.
[50] Chen, M. I., Branch, T. P., and Hutton, W. C., 1996, ''Is It Important to Secure the Horns During Lateral Meniscal Transplantation? A Cadaveric Study,'' Arthroscopy, **12**, pp. 174–181.
[51] Kadaba, M. P., Ramakrishnan, H. K., and Wootten, M. E., 1990, ''Measurement of Lower Extremity Kinematics During Level Walking,'' J. Orthop. Res., **8**, pp. 383–392.
[52] Lafortune, M. A., Cavanagh, P. R., Sommer, H. J., and Kalenak, A., 1992, ''Three-Dimensional Kinematics of the Human Knee During Walking,'' J. Biomech., **25**, pp. 347–357.
[53] Chao, E. Y., Laughman, R. K., Schneider, E., and Stauffer, R. N., 1983, ''Normative Data of Knee Joint Motion and Ground Reaction Forces in Adult Level Walking,'' J. Biomech., **16**, pp. 219–233.